



nature > nature nanotechnology > articles > article

Article | Published: 29 June 2020

Subretinally injected semiconducting polymer nanoparticles rescue vision in a rat model of retinal dystrophy

José Fernando Maya-Vetencourt, Giovanni Manfredi, Maurizio Mete, Elisabetta Colombo, Mattia Bramini, Stefano Di Marco, Dmytro Shmal, Giulia Mantero, Michele Dipalo, Anna Rocchi, Mattia L. DiFrancesco, Ermanno D. Papaleo, Angela Russo, Jonathan Barsotti, Cyril Eleftheriou, Francesca Di Maria, Vanessa Cossu, Fabio Piazza, Laura Emionite, Flavia Ticconi, Cecilia Marini, Gianmario Sambuceti, Grazia Pertile, Guglielmo Lanzani  & Fabio Benfenati 

Nature Nanotechnology **15**, 698–708(2020) | [Cite this article](#)

3280 Accesses | **1** Citations | **300** Altmetric | [Metrics](#)

Abstract

Inherited retinal dystrophies and late-stage age-related macular degeneration, for which treatments remain limited, are among the most prevalent causes of legal blindness. Retinal prostheses have been developed to stimulate the inner retinal network; however, lack of sensitivity and resolution, and the need for wiring or external cameras, have limited their application. Here we show that conjugated polymer nanoparticles (P3HT NPs) mediate light-evoked stimulation of retinal neurons and persistently rescue visual functions when subretinally injected in a rat model of retinitis pigmentosa. P3HT NPs spread out over the entire subretinal space and promote light-dependent activation of spared inner retinal neurons, recovering subcortical, cortical and behavioural visual responses in the absence of trophic effects or retinal inflammation. By conferring sustained light sensitivity to degenerate retinas after a single injection, and with the potential for high spatial resolution, P3HT NPs provide a new avenue in retinal prosthetics with potential applications not only in retinitis pigmentosa, but also in age-related macular degeneration.

Access options

Subscribe to Journal

Get full journal access for 1 year

\$169.00

only \$14.08 per issue

Subscribe

All prices are NET prices.

VAT will be added later in the checkout.

Rent or Buy article

Get time limited or full article access on ReadCube.

from \$8.99

Rent or Buy

All prices are NET prices.

Additional access options:

- [Login](#)
- [Access through your institution](#)
- [Learn about institutional subscriptions](#)

Data availability

The data that support the plots within this paper together with other findings of this study are available from the corresponding author upon reasonable request.

Code availability

Custom codes and software used in this paper can be obtained from the corresponding authors on request.

References

1. Pascolini, D. & Mariotti, S. P. Global estimates of visual impairment: 2010. *Br.J. Ophthalmol.* **9**, 614–618 (2012).

-
2. Provis, J. M., Penfold, P. L., Cornish, E. E., Sandercoe, T. M. & Madigan, M. C. Anatomy and development of the macula: specialization and the vulnerability to macular degeneration. *Clin. Exp. Optom.* **88**, 269–281 (2005).

[Google Scholar](#)

-
3. Ziccardi, L. et al. Gene therapy in retinal dystrophies. *Int. J. Mol. Sci.* **20**, 22 (2019).

[Google Scholar](#)

-
4. Maeda, A., Mandai, M. & Takahashi, M. Gene and induced pluripotent stem cell therapy for retinal diseases. *Annu. Rev. Genom. Hum. Genet.* **20**, 201–216 (2019).

[CAS](#) [Google Scholar](#)

-
5. Simunovic, M. P. et al. Optogenetic approaches to vision restoration. *Exp. Eye Res.* **178**, 15–26 (2019).

[CAS](#) [Google Scholar](#)

-
6. Scholl, H. P. et al. Emerging therapies for inherited retinal degeneration. *Sci. Transl. Med.* **8**, 368rv6 (2016).

[Google Scholar](#)

-
7. Benfenati, F. & Lanzani, G. New technologies for developing second generation retinal prostheses. *Lab Anim.* **47**, 71–75 (2018).

[Google Scholar](#)

-
8. Bloch, E., Luo, Y. & da Cruz, L. Advances in retinal prosthesis systems. *Ther. Adv. Ophthalmol.* **11**, 1–19 (2019).

[Google Scholar](#)

-
9. Dagnelie, G. et al. Performance of real-world functional vision tasks by blind subjects improves after implantation with the Argus® II retinal prosthesis system. *Clin. Exp. Ophthalmol.* **45**, 152–159 (2017).

[Google Scholar](#)

-
10. Stingl, K. et al. Artificial vision with wirelessly powered subretinal electronic implant alpha-IMS. *Proc. Biol. Sci.* **280**, 20130077 (2013).

-
11. Lorach, H. et al. Photovoltaic restoration of sight with high visual acuity. *Nat. Med.* **21**, 476–482 (2015).
[CAS](#) [Google Scholar](#)
-
12. Manfredi, G., Colombo, E., Barsotti, J., Benfenati, F. & Lanzani, G. Photochemistry of organic retinal prostheses. *Annu. Rev. Phys. Chem.* **70**, 99–121 (2019).
[CAS](#) [Google Scholar](#)
-
13. Rivnay, J., Wang, H., Fenno, L., Deisseroth, K. & Malliaras, G. G. Next-generation probes, particles, and proteins for neural interfacing. *Sci. Adv.* **3**, e1601649 (2017).
[Google Scholar](#)
-
14. Tian, B. et al. Roadmap on semiconductor-cell biointerfaces. *Phys. Biol.* **15**, 031002 (2018).
[Google Scholar](#)
-
15. Ghezzi, D. et al. A hybrid bioorganic interface for neuronal photoactivation. *Nat. Commun.* **2**, 166 (2011).
[Google Scholar](#)
-
16. Feyen, P. et al. Light-evoked hyperpolarization and silencing of neurons by conjugated polymers. *Sci. Rep.* **6**, 22718 (2016).
[CAS](#) [Google Scholar](#)
-
17. Ghezzi, D. et al. A polymer optoelectronic interface restores light sensitivity in blind rat retinas. *Nat. Photonics* **7**, 400–406 (2013).
[CAS](#) [Google Scholar](#)
-
18. Gautam, V., Rand, D., Hanein, Y. & Narayan, K. S. A polymer optoelectronic interface provides visual cues to a blind retina. *Adv. Mater.* **26**, 1751–1756 (2014).
[CAS](#) [Google Scholar](#)
-
19. Gal, A. et al. Mutations in MERTK, the human orthologue of the RCS rat retinal dystrophy gene, cause retinitis pigmentosa. *Nat. Genet.* **26**, 270–271 (2000).
[CAS](#) [Google Scholar](#)
-

20. Antognazza, M. R. et al. Characterization of a polymer-based fully organic prosthesis for implantation into the subretinal space of the rat. *Adv. Healthc. Mater.* **5**, 2271–2282 (2016).

[CAS](#) [Google Scholar](#)

21. Maya-Vetencourt, J. F. et al. A fully organic retinal prosthesis restores vision in a rat model of degenerative blindness. *Nat. Mater.* **16**, 681–689 (2017).

[CAS](#) [Google Scholar](#)

22. Rossi, E. A. & Roorda, A. The relationship between visual resolution and cone spacing in the human fovea. *Nat. Neurosci.* **13**, 156–157 (2010).

[CAS](#) [Google Scholar](#)

23. Di Maria, F., Lodola, F., Zucchetti, E., Benfenati, F. & Lanzani, G. The evolution of artificial light actuators in living systems: from planar to nanostructured interfaces. *Chem. Soc. Rev.* **47**, 4757–4780 (2018).

[Google Scholar](#)

24. Feng, L. et al. Conjugated polymer nanoparticles: preparation, properties, functionalization and biological applications. *Chem. Soc. Rev.* **42**, 6620–6633 (2013).

[CAS](#) [Google Scholar](#)

25. Colombo, E., Feyen, P., Antognazza, M. R., Lanzani, G. & Benfenati, F. Nanoparticles: a challenging vehicle for neural stimulation. *Front. Neurosci.* **10**, 105 (2016).

[Google Scholar](#)

26. Chen, S. et al. Near-infrared deep brain stimulation via upconversion nanoparticle-mediated optogenetics. *Science* **359**, 679–684 (2018).

[CAS](#) [Google Scholar](#)

27. Ma, Y. et al. Mammalian near-infrared image vision through injectable and self-powered retinal nanoantennae. *Cell* **177**, 243–255 (2019).

28. Tuncel, D. & Demir, H. V. Conjugated polymer nanoparticles. *Nanoscale* **2**, 484–494 (2010).

[CAS](#) [Google Scholar](#)

29. Zangoli, M. et al. Engineering thiophene-based nanoparticles to induce phototransduction in live cells under illumination. *Nanoscale* **9**, 9202–9209 (2017).
[CAS](#) [Google Scholar](#)
-
30. Pu, M., Xu, L. & Zhang, H. Visual response properties of retinal ganglion cells in the Royal College of Surgeons dystrophic rat. *Invest. Ophthalmol. Vis. Sci.* **47**, 3579–3585 (2006).
[Google Scholar](#)
-
31. Martino, N. et al. Photothermal cellular stimulation in functional bio-polymer interfaces. *Sci. Rep.* **5**, 8911 (2015).
[CAS](#) [Google Scholar](#)
-
32. Mosconi, E. et al. Surface polarization drives photo-induced charge separation at the P3HT/water interface. *ACS Energy Lett.* **1**, 454–463 (2016).
[CAS](#) [Google Scholar](#)
-
33. Fendyur, A., Mazurski, N., Shappir, J. & Spira, M. E. Formation of essential ultrastructural interface between cultured hippocampal cells and gold mushroom-shaped MEA—toward “IN-CELL” recordings from vertebrate neurons. *Front. Neuroeng.* **4**, 14 (2011).
[Google Scholar](#)
-
34. Shmoel, N. et al. Multisite electrophysiological recordings by self-assembled loose-patch-like junctions between cultured hippocampal neurons and mushroom-shaped microelectrodes. *Sci. Rep.* **6**, 27110 (2016).
[CAS](#) [Google Scholar](#)
-
35. Hanson, L., Lin, Z. C., Xie, C., Cui, Y. & Cui, B. Characterization of the cell-nanopillar interface by transmission electron microscopy. *Nano Lett.* **12**, 5815–5820 (2012).
[CAS](#) [Google Scholar](#)
-
36. Pardue, M. T. et al. Neuroprotective effect of subretinal implants in the RCS rat. *Invest. Ophthalmol. Vis. Sci.* **46**, 674–682 (2005).
[Google Scholar](#)
-
37. Morimoto, T. et al. Transcorneal electrical stimulation promotes the survival of

photoreceptors and preserves retinal function in Royal College of Surgeons rats. *Invest. Ophthalmol. Vis. Sci.* **48**, 4725–4732 (2007).

[Google Scholar](#)

38. Zhou, W. T. et al. Electrical stimulation ameliorates light-induced photoreceptor degeneration *in vitro* via suppressing the proinflammatory effect of microglia and enhancing the neurotrophic potential of Müller cells. *Exp. Neurol.* **238**, 192–208 (2012).

[CAS](#) [Google Scholar](#)

39. Lorach, H. et al. Long-term rescue of photoreceptors in a rodent model of Retinitis Pigmentosa associated with MERTK mutation. *Sci. Rep.* **8**, 11312 (2018).

[CAS](#) [Google Scholar](#)

40. LaVail, M. M. & Battelle, B. A. Influence of eye pigmentation and light deprivation on inherited retinal dystrophy in the rat. *Exp. Eye Res.* **21**, 167–192 (1975).

[CAS](#) [Google Scholar](#)

41. Lucas, R. J. et al. Diminished pupillary light reflex at high irradiances in melanopsin-knockout mice. *Science* **299**, 245–247 (2003).

[CAS](#) [Google Scholar](#)

42. Maya Vetencourt, J. F. et al. The antidepressant fluoxetine restores plasticity in the adult visual cortex. *Science* **320**, 385–388 (2008).

[CAS](#) [Google Scholar](#)

43. McGill, T. J., Douglas, R. M., Lund, R. D. & Prusky, G. T. Quantification of spatial vision in the Royal College of Surgeons rat. *Invest. Ophthalmol. Vis. Sci.* **45**, 932–936 (2004).

[Google Scholar](#)

44. Phelps, M. E. Positron computed tomography studies of cerebral glucose metabolism in man: theory and application in nuclear medicine. *Semin. Nucl. Med.* **11**, 32–49 (1981).

[CAS](#) [Google Scholar](#)

45. Hustinx, R., Smith, R. J., Benard, F., Bhatnagar, A. & Alavi, A. Can the standardized uptake value characterize primary brain tumors on FDG-PET? *Eur. J. Nucl. Med.* **26**, 1501–1509 (1999).

46. Bourin, M. & Hascoet, M. The mouse light/dark box test. *Eur. J. Pharm.* **463**, 55–65 (2003).

[CAS](#) [Google Scholar](#)

47. Smith, G. & Atchinson, D.A. in *The Eye and Visual Optical Instruments* pp 291–316 (Cambridge University Press, 1997).

48. Chen, J., Patil, S., Seal, S. & McGinnis, J. F. Rare earth nanoparticles prevent retinal degeneration induced by intracellular peroxides. *Nat. Nanotechnol.* **1**, 142–150 (2006).

[CAS](#) [Google Scholar](#)

49. Shapiro, M. G., Homma, K., Villarreal, S., Richter, C. P. & Bezanilla, F. Infrared light excites cells by changing their electrical capacitance. *Nat. Commun.* **3**, 736 (2012).

[Google Scholar](#)

50. Carvalho-de-Souza, J. L. et al. Photosensitivity of neurons enabled by cell-targeted gold nanoparticles. *Neuron* **86**, 207–217 (2015).

[CAS](#) [Google Scholar](#)

51. Barbarella, G., Bongini, A. & Zambianchi, M. Regiochemistry and conformation of poly(3-hexylthiophene) via the synthesis and the spectroscopic characterization of the model configurational triads. *Macromolecules* **27**, 3039–3045 (1994).

[CAS](#) [Google Scholar](#)

52. Shimizu, H., Yamada, M., Wada, R. & Okabe, M. Preparation and characterization of water self-dispersible poly(3-hexylthiophene) particles. *Polym. J.* **40**, 33–36 (2007).

[Google Scholar](#)

53. Santoro, F. et al. Revealing the cell-material interface with nanometer resolution by focused ion beam/scanning electron microscopy. *ACS Nano* **11**, 8320–8328 (2017).

[CAS](#) [Google Scholar](#)

54. Pizzorusso, T. et al. Structural and functional recovery from early monocular deprivation in adult rats. *Proc. Natl Acad. Sci. U. S. A.* **103**, 8517–8522 (2006).

[CAS](#) [Google Scholar](#)

-
55. Maya-Vetencourt, J. F. et al. Experience-dependent expression of NPAS4 regulates plasticity in adult visual cortex. *J. Physiol.* **590**, 4777–4787 (2012).
[CAS](#) [Google Scholar](#)
-
56. Huang, Z. J. et al. BDNF regulates the maturation of inhibition and the critical period of plasticity in mouse visual cortex. *Cell* **98**, 739–755 (1999).
[CAS](#) [Google Scholar](#)
-
57. Porciatti, V., Pizzorusso, T. & Maffei, L. The visual physiology of the wild type mouse determined with pattern VEPs. *Vis. Res.* **39**, 3071–3081 (1999).
[CAS](#) [Google Scholar](#)
-
58. Porciatti, V., Pizzorusso, T. & Maffei, L. Electrophysiology of the postreceptoral visual pathway in mice. *Doc. Ophthalmol.* **104**, 69–82 (2002).
[Google Scholar](#)
-
59. Krzywinski, M. & Altman, N. Power and sample size. *Nat. Methods* **10**, 1139–1140 (2013).
[CAS](#) [Google Scholar](#)
-
60. Pedregosa, F. et al. Scikit-learn: machine learning in Python. *J. Mach. Learn. Res.* **12**, 2825–2830 (2011).
[Google Scholar](#)
-
61. Pitman, E. J. G. Significance tests which may be applied to samples from any populations. *J. R. Stat. Soc.* **4**(Suppl.), 119 (1937).
-
62. Hunter, J. D. Matplotlib: a 2D graphics environment. *Comput. Sci. Eng.* **9**, 90–95 (2007).
[Google Scholar](#)
-

[Download references](#) 

Acknowledgements

We thank M. M. La Vail (Beckman Vision Centre, University of California San Francisco) for providing non-dystrophic RCS-rdy+ and dystrophic RCS rats, N. De Petrocellis and N. Forte (CNR Institute for Biomolecular Chemistry) for stably hTRPV1-transfected HEK293 clones, E. Lingueglia (CNRS Institute of Molecular and Cellular Pharmacology) for providing the complementary DNA for the ASIC1a channel, A. Desii, S. Francia and M. Salerno (Istituto Italiano di Tecnologia) for help in the preparation and characterization of NPs, M. Cilli and A. Buschiazzo (IRCCS Ospedale Policlinico San Martino) for assistance in the surgical procedures and help in positron emission tomography imaging and R. Ciancio, I. Dallorto, A. Mehilli, R. Navone and D. Moruzzo (Istituto Italiano di Tecnologia) for technical assistance. The work was supported by the Italian Ministry of Health (project RF-2013-02358313 to G.P., G.L. and F.B.), Fondazione Cariplo (project 2018-0505 to G.L., F.B. and G.P.), Compagnia di San Paolo (project 9798 to J.F.M.-V.), H2020-MSCA-ITN 2019 “Entrain Vision” (project 861423 to F.B.) and EuroNanoMed3 (project 2019-132 “NanoLight” to F.B.). The support of the Ra.Mo. Foundation, Rare Partners srl and Fondazione 13 Marzo is also acknowledged.

Author information

Mattia Bramini

Present address: Department of Applied Physics, University of Granada, Granada, Spain

Cyril Eleftheriou

Present address: Departments of Ophthalmology and Neurology, Weil Medical College of Cornell University, White Plains, NY, USA

Flavia Ticconi

Present address: Department of Oncohematology, Nuclear Medicine Unit, Faenza Hospital, Faenza, Italy

Affiliations

Centre for Synaptic Neuroscience and Technology, Istituto Italiano di Tecnologia, Genoa, Italy

José Fernando Maya-Vetencourt, Elisabetta Colombo, Mattia Bramini, Stefano Di Marco, Dmytro Shmal, Giulia Mantero, Anna Rocchi, Mattia L. DiFrancesco, Ermanno D. Papaleo, Cyril Eleftheriou & Fabio Benfenati

IRCCS Ospedale Policlinico San Martino, Genoa, Italy

José Fernando Maya-Vetencourt, Elisabetta Colombo, Stefano Di Marco, Anna Rocchi, Vanessa Cossu, Laura Emionite, Flavia Ticconi, Gianmario Sambuceti & Fabio Benfenati

Department of Biology, University of Pisa, Pisa, Italy

José Fernando Maya-Vetencourt

Centre for Nano Science and Technology, Istituto Italiano di Tecnologia, Milan, Italy

Giovanni Manfredi, Jonathan Barsotti & Guglielmo Lanzani

Ophthalmology Department, IRCCS Ospedale Sacro Cuore Don Calabria, Negrar, Italy

Maurizio Mete, Angela Russo & Grazia Pertile

Plasmon Nanotechnologies, Istituto Italiano di Tecnologia, Genoa, Italy

Michele Dipalo

CNR Institute of Organic Synthesis and Photoreactivity (ISOF), Bologna, Italy

Francesca Di Maria

Department of Health Science, Nuclear Medicine, University of Genoa, Genoa, Italy

Vanessa Cossu, Flavia Ticconi & Gianmario Sambuceti

ENT Department, ASST Mantova, Mantua, Italy

Fabio Piazza

CNR Institute of Bioimages and Molecular Physiology, Milan (Genoa Section), Genoa, Italy

Cecilia Marini

Department of Physics, Politecnico di Milano, Milan, Italy

Guglielmo Lanzani

Contributions

J.F.M.-V. followed all in vivo experiments by performing electrophysiology and behavioural analyses under the supervision of F.B. and assisted in the optical coherence tomography and positron emission tomography trials; G.P., M.M. and A. Russo developed and executed the subretinal microinjection; M.M. performed optical coherence tomography analysis; G. Manfredi, J.B. and F.D.M. fabricated the NPs and characterized them under the supervision of G.L.; E.C., S.D.M., M.L.D., E.D.P., M.D. and M.B. performed the in vitro/ex vivo electrophysiological and EM experiments on HEK cells, neurons and retinal explants under the supervision of F.B.; V.C., F.T., L.E., D.S. and C.M. executed positron emission tomography experiments under the supervision of G.S.; D.S., G. Mantero and C.E. performed histological analyses under the supervision of S.D.M. and J.F.M.-V.; A. Rocchi performed the qRT-PCR experiments; J.F.M.-V., G.L. and F.B. wrote the manuscript; F.P. revised the manuscript; F.B., G.P., J.F.M.-V. and G.L. conceived, supervised and financed the project. All authors discussed the experimental results and commented on the manuscript.

Corresponding authors

Correspondence to [Guglielmo Lanzani](#) or [Fabio Benfenati](#).

Ethics declarations

Competing interests

The P3HT NPs studied in this paper are the subject of the US patent application US 16/005248 'Eye-injectable polymeric nanoparticles and method of use therefor' by Istituto Italiano di Tecnologia and Ospedale Sacrocuore Don Calabria, with J.F.M.-V., M.M., G.P., F.B. and G.L. as inventors. The other authors declare no competing interests.

Additional information

Publisher's note Springer Nature remains neutral with regard to jurisdictional claims in published maps and institutional affiliations.

Extended data

Extended Data Fig. 1 P3HT nanoparticles incubated with primary neurons are not internalized.

a, Primary cortical neurons exposed to P3HT-NPs for 1 h were live stained with Cell Mask and analysed by confocal imaging. Cell Mask (cyan) labels the neuronal membrane, bisbenzimidazole (blue) highlights cell nuclei and the intrinsic P3HT fluorescence (red) visualizes NPs. In the middle panel, a higher magnification image of the neuron shows the co-localization of P3HT-NPs with the membrane (pink overlaid areas). The results are representative of $n = 3$ independent neuronal preparations. **b**, To quantify NP internalization, neurons were exposed to P3HT-NPs for either 1 h (shown) or 1 week (not shown) fixed, double immunostained for β III-tubulin (blue) and the specific lysosomal marker LAMP1 (green) and analysed by confocal microscopy. **c**, Box plot of the extent of NPs/LAMP1 co-localization, quantified by acquiring 3D z-stack confocal images. The median P3HT NPs/LAMP1 volume ratios were 1.65% and 1.75% for 1-h and 1-week incubations, respectively. Box plots represent the median (centre line), mean (square), 25th-75th percentiles (box) and the limit of 3-fold the interquartile range. Sample size: $n = 22$ neurons from 2 independent neuronal preparations. Scale bars, 20 μ m (main images); 5 μ m (zoomed images).

Extended Data Fig. 2 Quantification of cell bodies in the ONL of dystrophic RCS rats at 30 and 240 DPI.

The boundaries of the avascular ONL were determined in transversal sections of representative healthy and dystrophic retinas dissected at 30 DPI (**a**) and 240 DPI (**c**) by histochemistry with isolectin GS-IB4 (red) staining retinal and choroidal vessels, combined

with cell nuclear staining with bisbenzimidazole (blue). A clear-cut thinning of the ONL associated with widening of the INL was present at both 30 DPI and 240 DPI. Quantification of the number of cell layers labelled with bisbenzimidazole in the ONL revealed a massive decrease of the nuclear rows of photoreceptors in all dystrophic retinas (non-injected, P3HT-NP injected or sham Glass-NP injected) already at 30 DPI (4 months-old rats; **b**), that further progressed at 240 DPI (11 months-old rats; **d**). Means \pm sem are shown together with dots representing the mean value obtained for each animal from 9 samplings (3 samples/field and 3 fields/retina). *** $p < 0.001$, one-way ANOVA/Bonferroni's tests. Data are means \pm sem with superimposed individual experimental points. Sample size (experimental animals) @ 30 DPI: RCS-rdy, $n = 13$; RCS, $n = 13$; RCS + P3HT, $n = 11$; RCS + Glass, $n = 14$. Sample size (experimental animals) @ 240 DPI: RCS-rdy, $n = 9$; RCS, $n = 9$; RCS + P3HT, $n = 8$; RCS + Glass, $n = 10$. For exact p values, see Supplementary Table 3. ONL, outer nuclear layer; INL, inner nuclear layer; GCL, ganglion cell layer. Scale bar, 100 μm .

Extended Data Fig. 3 Degeneration in dystrophic RCS retinas selectively hits recoverin-positive photoreceptors in the ONL.

a, Representative image of a retina section from $n = 5$ non-dystrophic RCS-rdy rats (4 months-old) stained with bisbenzimidazole to localize cell nuclei (red; *left panel*) and recoverin staining (white; *right panel*) to highlight both photoreceptor (pink arrows) and bipolar (green arrows) cell bodies. **b**, The frequency distribution of the cell diameter in non-dystrophic RCS-rdy retinas shows a bimodal pattern that allows distinguishing between photoreceptor (mean \pm sem: $5.73 \pm 0.78 \mu\text{m}$) and bipolar (mean \pm sem: $12.15 \pm 0.14 \mu\text{m}$) cell bodies. All 4 months-old dystrophic RCS groups, no matter whether treated (30 DPI) or untreated, show a single distribution of cell diameters around 12 μm , coinciding with that of bipolar cells in RCS-rdy. This shows that photoreceptors are dramatically decreased in all groups of RCS rats, while recoverin-positive bipolar cells are relatively unaffected. **c**, Pie charts representing the relative number of recoverin-positive photoreceptors and recoverin positive-bipolar cells expressed in percentage of the total cell body counts in control RCS-rdy retinas. The white areas in the RCS groups represent the percentage of photoreceptor loss. Sample size in **b,c** (experimental animals): $n = 5$ per experimental group (30 DPI). For each animal, images were acquired from corresponding fields in the various retinas by taking the injection site as reference point (2 slices/retina; 3 fields/slice). ONL, outer nuclear layer; INL, inner nuclear layer; GCL, ganglion cell layer. Scale bar, 50 μm .

Extended Data Fig. 4 Expression of photoreceptor-specific mRNAs in the retina of RCS rats at 30 and 240 DPI.

The mRNA levels of Rhodopsin (*Rho*; **a**), Opsin-1 short wave-sensitive (*Opn1sw*; **b**) and Opsin-1 medium wave-sensitive (*Opn1mw*; **c**) were quantified by qRT-PCR in retinal sections dissected from non-dystrophic controls (RCS-rdy) and dystrophic RCS rats that were non-injected (RCS) or injected with either P3HT-NPs or control Glass-NPs at 30 and 240 DPI. *Gapdh* and *HPRT1* were used as control housekeeping genes. Graphs show means \pm sem on a semilogarithmic scale with superimposed individual points. Sample size (experimental animals): RCS-rdy (blue), $n = 4$; RCS

(green), $n = 4$; RCS + P3HT (red), $n = 4$; RCS + Glass (orange), $n = 4$ for 30 and 240 DPI groups. $**p < 0.01$, $***p < 0.0001$, one-way ANOVA/Newman-Keuls tests *vs* the respective RCS-rdy group. For exact p values, see Supplementary Table 3.

Extended Data Fig. 5 P3HT nanoparticles do not promote proinflammatory effects in dystrophic retinas.

Transversal sections of representative retinas dissected at 30 DPI (a–c) and 240 DPI (d–f) from healthy controls (RCS-rdy) and dystrophic RCS rats that were untreated (RCS) or injected with either P3HT-NPs (RCS + P3HT) or control Glass-NPs (RCS + Glass). Sections were immunolabelled for: the astrocyte/Müller cell marker GFAP (a,d), the microglial marker Iba-1 (b,e) and the retinal trophic factor FGF2 (c,f). Images were acquired from corresponding fields in the various retinas by taking the injection site as reference point (2 slices/retina; 3 fields/slice). Immunostainings were merged with bisbenzimidazole nuclear labelling (blue). The bar plots on the right (means \pm sem with superimposed individual data points) report the quantitative analysis of the integrated fluorescence intensity. Dystrophic retinas display higher densities of activated astrocytes, microglial cells and FGF2-positive cells compared to RCS-rdy, as a result of the ongoing degeneration. All the RCS groups show a similar density of GFAP/Iba-1/FGF2 positive cells demonstrating that the presence of either P3HT-NPs or Glass-NPs did not promote a significant tissue inflammatory reaction. $*** p < 0.001$, $**** p > 0.0001$, *vs* RCS-rdy controls; one-way ANOVA/Dunnett's tests. Sample size (experimental animals) @ 30 DPI: GFAP 11, 10, 10, 11; Iba-1 11, 12, 12, 12; FGF2 8, 7, 7, 8; for RCSrdy, RCS, RCS + P3HT and RCS + Glass, respectively. Sample size (experimental animals) @ 240 DPI: GFAP 7, 6, 6, 7; Iba-1 8, 9, 8, 8; FGF2 4, 4, 4, 4; for RCSrdy, RCS, RCS + P3HT and RCS + Glass, respectively). For exact p values, see Supplementary Table 3. ONL, outer nuclear layer; INL, inner nuclear layer; GCL, ganglion cell layer. Scale bar, 50 μ m.

Extended Data Fig. 6 VEP latency in RCS rats.

a, Latency of VEPs evoked by white light flashes at 30 and 240 DPI. The electrophysiological analysis revealed that the VEP latency in RCS-rdy animals was significantly lower compared to that of RCS, RCS + P3HT-NPs or RCS + Glass-NPs at 30 DPI. The same phenomenon, albeit more pronounced, was observed at 240 DPI. The greatly increased VEP latency in aged dystrophic RCS rats is likely due to the extensive retinal rewiring that follows photoreceptor degeneration. Notably, the increased latency of dystrophic RCS rats is not rescued by P3HT-NPs at both 30 and 240 DPI. Data are means \pm sem. $** p < 0.01$; $*** p < 0.001$ *vs* RCS-rdy controls at 30 and 240 DPI, respectively; one-way ANOVA/Tukey's tests. Sample size (experimental animals) @ 30 DPI: RCS-rdy, $n = 8$; RCS, $n = 7$; RCS + P3HT-NPs, $n = 12$; RCS + Glass-NPs, $n = 6$. Sample size (experimental animals) @ 240 DPI: $n = 4$ per each experimental group. **b**, Latency of VEPs evoked by white (W) or red (R) light flashes at 30 DPI from the experiment shown in Fig. 5h. No VI response to red stimuli was detected in healthy RCS-rdy rats (indicated as infinite latency). The VEP latencies to white and red light of dystrophic RCS rats injected with P3HT-NPs were not significantly different, while they were both significantly longer than the VEP latency to white

light of healthy RCS-rdy rats. **** $p < 0.0001$; NS $p > 0.05$; one-way ANOVA/Tukey's tests. Data are means \pm sem with superimposed individual experimental points. Sample size (experimental animals): RCS-rdy, $n = 8$; RCS + P3HT-NPs, $n = 7$. For exact p values, see Supplementary Table 3.

Extended Data Fig. 7 Light-evoked metabolic activation of V1 is rescued in dystrophic RCS rats injected with P3HT nanoparticles.

a, Representative brain images of basal metabolic activity acquired in the four experimental groups at 240 DPI. A map of the rat brain showing the location of V1 (blue areas) and a pseudo-colour scale corresponding to the average SUV of ^{18}F -FDG uptake over the scanned areas are shown on the left. **b**, Quantitative analysis of the average SUV in the V1 volumes of interest ($\sim 1 \text{ mm}^3$) demonstrates a significant increase in light evoked V1 metabolic activity in RCS rats injected with P3HT-NPs at 240 DPI. Box plots in **b** represent the median (centre line), mean (square), 25th-75th percentiles (box) and the limit of 3-fold the interquartile range. * $p < 0.05$; ** $p < 0.01$; one-way ANOVA/Tukey's tests. Sample size (experimental animals): RCS-rdy, $n = 10$; RCS, $n = 12$; RCS + P3HT-NPs, $n = 14$; RCS + glass-NPs, $n = 11$. For exact p values, see Supplementary Table 3.

Extended Data Fig. 8 Correlation map of all the variables studied in the four experimental groups of RCS rats.

Each column and each row describe a different variable, with squares on the map representing the correlation between row and column variables ("photoreceptor", "inflammation" and "visual function" variables). Analysis by the Pearson's correlation coefficient revealed the existence of a strong correlation among all the variables, suggesting the use of a Principal Component Analysis decomposition. Sample size (experimental animals) @ 30 DPI: RCS-rdy, $n = 5$; RCS, $n = 5$; RCS + P3HT-NPs, $n = 5$; RCS + Glass-NPs, $n = 6$. Sample size (experimental animals) @ 240 DPI: RCS-rdy, $n = 4$; RCS, $n = 4$; RCS + P3HT-NPs, $n = 4$; RCS + Glass-NPs, $n = 4$. PLR, pupillary constriction; VEPs, VEP amplitude; GFAP, astrocyte immunoreactivity; IBA-1, microglia immunoreactivity; FGF2, fibroblast growth factor immunoreactivity; PhRecCounts, recoverin-positive photoreceptor cell bodies; ConesCounts, cone arrestin-positive cone cell bodies; ONL cell rows, bisbenzimidazole-stained nuclear rows in the ONL; Acuity, visual acuity; Dark persistence, percentage time in the dark in the light-dark box behavioural test.

Extended Data Fig. 9 Component analysis for morphological and functional parameters in individual animals at 30 and 240 DPI.

3D plot of RCS morphological and functional parameters as a function of 3 reduced variables at 30 and 240 DPI. The x , y , z variables are indicators of visual performances (PLR, VEPs, Acuity, Dark persistence), photoreceptor cell counts (rod, cone and cell rows in the ONL, as reported in Supplementary Fig. 14) and the inflammatory state of the retina (GFAP, Iba-1 and FGF2 immunoreactivities, as reported in Supplementary Fig. 15), respectively. The scatter plots report the individual responses at 30 (**a**) and 240 (**b**) DPI within the four experimental groups. The shaded areas represent the highest values (up to 0.001) of the probability density function of the calculated clusters. The dashed lines and their terminal points represent the projections

of each cluster centroid onto the origin planes. Sample size (experimental animals) @ 30 DPI: RCS-rdy (blue; n = 5), RCS (green; n = 5), RCS + P3HT-NPs (red; n = 5) and RCS + Glass-NPs (orange; n = 6). Sample size (experimental animals) @ 240 DPI: RCS-rdy (blue; n = 4), RCS (green; n = 4), RCS + P3HT-NPs (red; n = 4) and RCS + Glass-NPs (orange; n = 4).

Supplementary information

Supplementary Information

Supplementary text, Tables 1–3, Figs. 1–16 and refs. 1–17.

Reporting Summary

Supplementary Video 1

Pupillary reflexes in bilaterally injected and dark-adapted animals at 30 DPI evoked by a light stimulus of 5 lux. Videos are image sequences obtained with a Hamamatsu camera at 5 Hz frame rate. Representative examples of the four experimental groups (RCS-rdy; RCS; RCS + P3HT NPs; RCS + glass NPs) are shown.

Supplementary Video 2

Pupillary reflexes in bilaterally injected and dark-adapted animals at 240 DPI evoked by a light stimulus of 5 lux. For further details, see caption to Supplementary Video 1.

Supplementary Video 3

Escape latency in the light–dark box test at 30 DPI. A representative example of the light (5 lux)-evoked escape behaviour is shown for each experimental group (RCS-rdy; RCS; RCS + P3HT NPs; RCS + glass NPs).

Supplementary Video 4

Escape latency in the light–dark box test at 240 DPI. For further details, see caption to Supplementary Video 3.

Rights and permissions

Reprints and Permissions

About this article



Check for
updates

Cite this article

Maya-Vetencourt, J.F., Manfredi, G., Mete, M. *et al.* Subretinally injected semiconducting polymer nanoparticles rescue vision in a rat model of retinal dystrophy. *Nat. Nanotechnol.* **15**, 698–708 (2020). <https://doi.org/10.1038/s41565-020-0696-3>

[Download citation](#) 

Received

21 January 2019

Accepted

20 April 2020

Published

29 June 2020

Issue Date

August 2020

DOI

<https://doi.org/10.1038/s41565-020-0696-3>

Subjects

Biotechnology

Materials science

Nanoscience and technology

Optics and photonics

Further reading

[A liquid retinal prosthesis](#)

Christine Horejs

Nature Reviews Materials (2020)

Nature Nanotechnology | ISSN 1748-3395 (online)

nature research

[About us](#) [Press releases](#) [Press office](#) [Contact us](#)



Discover content

Journals A-Z
Articles by subject
Nano
Protocol Exchange
Nature Index

Researcher services

Research data
Language editing
Scientific editing
Nature Masterclasses
Nature Research Academies

Advertising & partnerships

Advertising
Partnerships & Services
Media kits
Branded content

Regional websites

Nature China
Nature India
Nature Japan
Nature Korea
Nature Middle East

Publish with us

Guide to Authors
Guide to Referees
Editorial policies
Open access
Reprints & permissions

Libraries & institutions

Librarian service & tools
Librarian portal
Open research

Career development

Nature Careers
Nature Conferences
Nature events

Legal & Privacy

Privacy Policy
Use of cookies
Manage cookies/Do not sell my data
Legal notice
Accessibility statement
Terms & Conditions
California Privacy Statement

SPRINGER NATURE

© 2020 Springer Nature Limited